nature microbiology

ARTICLES

https://doi.org/10.1038/s41564-019-0379-8

Social evolution of innate immunity evasion in a virus

Pilar Domingo-Calap, Ernesto Segredo-Otero, María Durán-Moreno and Rafael Sanjuán*

Antiviral immunity has been studied extensively from the perspective of virus–cell interactions, yet the role of virus–virus interactions remains poorly addressed. Here, we demonstrate that viral escape from interferon (IFN)-based innate immunity is a social process in which IFN-stimulating viruses determine the fitness of neighbouring viruses. We propose a general and simple social evolution framework to analyse how natural selection acts on IFN shutdown and validate it in cell cultures and mice infected with vesicular stomatitis virus. Furthermore, we find that IFN shutdown is costly because it reduces short-term viral progeny production, thus fulfilling the definition of an altruistic trait. Hence, in well-mixed populations, the IFN-blocking wild-type virus is susceptible to invasion by IFN-stimulating variants and spatial structure consequently determines whether IFN shutdown can evolve. Our findings reveal that fundamental social evolution rules govern viral innate immunity evasion and virulence and suggest possible antiviral interventions.

Social interactions have shaped the evolution of organisms from bacteria to animals. Social evolution has been investigated using various approaches including kin selection, group selection and game theory[1–3], but has been seldom validated empirically in viruses[4]. Our lack of mechanistic understanding of how social interactions take place in viruses has been a major limitation. For instance, a landmark study showed that experimental populations of bacteriophages obey the prisoner's dilemma[5], but the underlying mechanisms were not elucidated. More recently, it was suggested that hepatitis C virus undergoes so-called antigenic cooperation, whereby virus variants eliciting broad cross-reactive antibodies facilitate the persistence of other variants[6]. However, the details of such interactions were not clarified.

Some molecular processes that potentially allow for social interactions among viruses have been characterized. For instance, certain phages secrete a short peptide that signals viral population density and guides lysis–lysogeny decisions[7] and some phage-encoded proteins partially antagonize but do not fully suppress anti-phage clustered regularly interspaced short palindromic repeats (CRISPRs), which might allow for cooperation if co- or super-infecting phages add together the effects of their proteins[8]. Potentially cooperative interactions have also been reported between neuraminidase variants of the influenza virus[9]. However, the social evolution of these virus–virus interactions has not been explored. More generally, bottom-up approaches that link specific molecular mechanisms to population-level processes are needed to achieve a better understanding of social evolution, not just in viruses but also in other types of organisms[10,11].

Innate immunity is the first line of defence against viruses; it is triggered by the recognition of pathogen-associated molecular patterns leading to the secretion of type-I interferons (IFNs) and other pro-inflammatory cytokines[12,13]. IFNs function in an autocrine manner, by self-inducing antiviral responses in the infected cell, and also in a paracrine manner, by signalling the infection locally and inducing a virus-resistant state in neighbouring cells. In response, viruses have evolved various mechanisms to suppress IFN-mediated innate immunity[13–15]. We propose that the ability of a given virus to suppress IFN-mediated innate immunity modifies the fitness of other members of the viral population and, thus, is a social trait. Specifically, we predict that variants failing to prevent IFN secretion spark antiviral responses that inhibit the spread of neighbouring viruses. We first model this process by partitioning viral fitness according to social neighbourhood. This shows that the condition for IFN shutdown to evolve is analogous to the classical Hamilton's rule[3]. We then demonstrate the social nature of IFN evasion in cell cultures and mice using IFN-stimulating and IFN-blocking vesicular stomatitis virus (VSV) variants.

Theory

We consider two virus variants, one that blocks IFN secretion (W) and another that does not (D), and partition the fitness of each variant according to its social neighbourhood. In particular, we call $f_{W|W}$ and $f_{W|D}$ the log-fitness of the W variant in a W neighbourhood and a D neighbourhood, respectively. Analogously, D fitness is partitioned into $f_{D|D}$ and $f_{W|D}$. For both variants, being in a W neighbourhood has a positive effect b relative to being in a D neighbourhood because IFN is not released from neighbouring cells. Hence, b is determined by paracrine IFN action and measures indirect fitness effects. On the other hand, c is the direct effect on the actor virus of blocking IFN, independent of neighbourhood. Blocking IFN secretion may provide a direct benefit through autocrine effects ($c<0$), but may also entail costs ($c>0$). We set the W virus in a W background as reference, such that $f_{W|W}=0$. By definition, then, $f_{W|D}=-b$, $f_{D|W}=c$ and $f_{D|D}=c-b$ (Fig. 1). We define W fitness across neighbourhoods as $f_W=r_W f_{W|W}+(1-r_W)f_{W|D}$, where r_W is a parameter indicating how strongly W is influenced by neighbouring viruses of its own type ($0\leq r_W\leq 1$). Analogously, $f_D=r_D f_{D|D}+(1-r_D)f_{D|W}$. Hence, $f_W=-b(1-r_W)$ and $f_D=r_D(c-b)+c(1-r_D)=c-r_D b$. Whether IFN suppression is favoured by selection depends on the quantity f_W-f_D, which equals $(r_W+r_D-1)b-c$.

We thus model IFN shutdown as a potentially costly, cooperative trait that is favoured by selection only if $(r_W+r_D-1)b-c>0$. By denoting $r=r_W+r_D-1$, we recover Hamilton's rule, $rb-c>0$, a central result of kin selection theory[3]. Hence, r may be interpreted

Institute for Integrative Systems Biology, Universitat de València–Consejo Superior de Investigaciones Científicas, Paterna, Spain.
*e-mail: rafael.sanjuan@uv.es

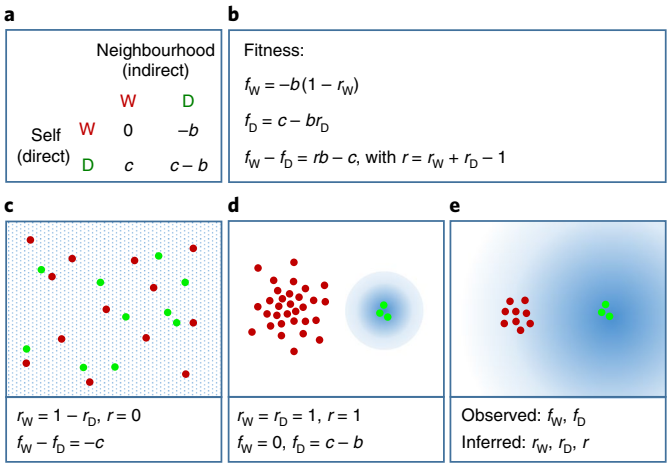

Fig. 1 | Social evolution model for innate immunity evasion. a, The partition of individual fitness according to social neighbourhood. One virus blocks IFN (W) and another does not (D). The W virus in a W neighbourhood is used as the reference and has $f = 0$. IFN-mediated paracrine signalling has an indirect fitness effect b that is applicable to W and D. The direct effect of blocking IFN on the actor, independent of neighbourhood effects, is denoted c, and can a priori be positive or negative. Because fitness is defined logarithmically, independent effects are additive and hence the fitness of D in a D neighbourhood is $c - b$. **b**, The fitness of each variant, which depends on spatial structure through r_W and r_D. **c**–**e**, Three possible scenarios (W-infected cells in red; D-infected cells in green; region of immunized cells in blue). **c**, No spatial structure, both viruses share the same neighbourhood. The dotted background indicates region of immunized cells. **d**, Maximal spatial structure. Analysis of these two cases allows b and c to be obtained. **e**, An intermediate situation. If f_W and f_D are measured and b and c are known, r_W, r_D and r can be inferred.

as a measure of genetic relatedness. However, here r is more precisely defined as the difference between the social neighbourhoods of W and D and describes spatial structure in terms of the immune response each variant receives. This spatial structure can vary from a loose assortment determined by IFN and viral diffusion to well-defined, isolated subpopulations. The effect of spatial structure on social evolution could also be modelled from a group selection perspective[16,17], which is generally accepted to be formally equivalent to kin selection[16–19]. A particularity of this system is that the social process is mediated by a diffusible antiviral protein. Therefore, IFN acts in a manner opposed to classical public goods, for example, secreted enzymes[20–22]. Suppressing IFN secretion creates a space that is favourable for viral growth, analogous to preventing the release of a pollutant. However, the presence of IFN-stimulating neighbours could render cooperation ineffective. We therefore expect the D variant to exert a strongly negative effect on W, whereas the W variant may provide little benefit to D. In terms of the model, this prediction is stated as $r_D > r_W$. Finally, we note that demography is not explicitly implemented in the model and that, consequently, changes in the size and structure of the viral population or the immune response may result in time-dependent parameters.

Interaction between WT and IFN-inducer VSV variants

To test the social nature of IFN shutdown empirically we used VSV, a prototypic negative-strand RNA animal virus. The VSV matrix protein M suppresses host gene expression, preventing IFN production[23]. Mutations in M at methionine 51 inactivate this function and attenuate VSV in IFN-competent cells[24,25]. Here, we used a deletion mutant (Δ51) carrying a green fluorescent protein (GFP) reporter and an isogenic wild-type (WT) virus carrying an mCherry reporter. Confirming previous work, we found by enzyme-linked immunosorbent assay (ELISA) that mouse embryonic fibroblasts (MEFs) inoculated with the Δ51 virus at a multiplicity of infection (MOI) of 3 foci forming units (FFU) per cell secreted IFN-β extensively (1,797 ± 108 units at 16 h post inoculation (hpi); error terms indicate the s.e.m.), whereas IFN remained undetectable in WT-infected cells. Similarly, mRNA levels of the IFN-stimulated anti-VSV effector Mx2 were 114.3 ± 8.1 times higher in MEFs infected with Δ51 than in those infected with WT.

Pure WT infections reached a final titre of 10^8 FFU ml^{-1} independent of the MOI at inoculation, whereas pure Δ51 infections reached a titre 10 to 200 times lower depending on the MOI (Fig. 2a). In MEFs infected with both variants, the total viral yield decreased exponentially with the fraction of Δ51 at inoculation (Fig. 2b), indicating that WT fitness was adversely affected by Δ51. To show the involvement of cytokines in this interaction, we filtered the supernatant from a Δ51 infection to remove virions and collect small proteins including IFNs. Pretreatment of cells with this conditioned medium inhibited WT growth strongly and in a dose-dependent manner (Fig. 2c). This effect became weaker if the virus and the conditioned medium were added simultaneously, and was nearly lost if the conditioned medium was added >3 hpi (Fig. 2d). Hence, the ability of IFN to suppress virus production in already-infected cells was limited, indicating that the role of IFN consisted mainly of protecting uninfected cells.

Spatial structure of infection and immunity

We first measured the area of influence of individual Δ51-infected cells. For this, we inoculated MEFs with Δ51–GFP at low MOI (<0.001 FFU cell^{-1}) and added a neutralizing monoclonal antibody (NmAb) following virus adsorption to prevent secondary infections. At 20 hpi, we added NmAb-resistant WT–mCherry virus (10 FFU cell^{-1}). This WT infected the entire culture except areas around Δ51-infected cells, which remained free of either virus (Fig. 2e). Therefore, Δ51 produced a spatially structured, negative influence on infection. We next used real-time fluorescence microscopy to investigate the spatial structure and dynamics of viral spread. To accomplish this, we performed pure and mixed (1:1 input) infections using WT and/or Δ51 variants (~0.01 FFU cell^{-1}). Both viruses completed the first infection cycle and reached neighbouring cells but whereas pure WT infections progressed further until invading the entire culture, Δ51 infections were halted at around 20 hpi (Fig. 3; Supplementary Fig. 1; Supplementary Videos 1 and 2). This is consistent with a delayed but effective onset of innate immunity, as shown previously[26,27]. At the end-point (43 hpi), pure WT infections infected 16.7 times more cells than pure Δ51 infections. Confirming the interference shown above, in mixed infections the spread of the WT was severely reduced, although it still reached 1.26 ± 0.09 more cells than Δ51 at 43 hpi (two-tailed t-test: $P = 0.058$; Fig. 3; Supplementary Fig. 1; Supplementary Video 3).

Altruistic nature of IFN shutdown

Initially, Δ51 spread more efficiently than the WT, reaching 2.43 more cells at 20 hpi. This was not explained by differences between the GFP and mCherry reporters (Supplementary Fig. 2). Furthermore, parallel infections of pure WT versus Δ51 viruses bearing the same GFP reporter confirmed the short-term advantage of Δ51 (Fig. 4a). Thus, before the onset of an effective innate immune response, IFN blockade was costly ($c > 0$). To quantify this cost, we disrupted spatial structure, such that r was minimal and hence $f_W - f_D \approx -c$. For this, we shuffled the cell monolayer twice (8 and 24 hpi) using trypsin, a treatment that should not affect IFN-mediated immunity[28]. Strikingly, under these conditions Δ51 outcompeted the WT, reaching 2.49 ± 0.18 times more cells at 43 hpi (t-test: $P = 0.001$; Fig. 3). To verify this result, we performed competition assays on the two variants over three serial transfers in

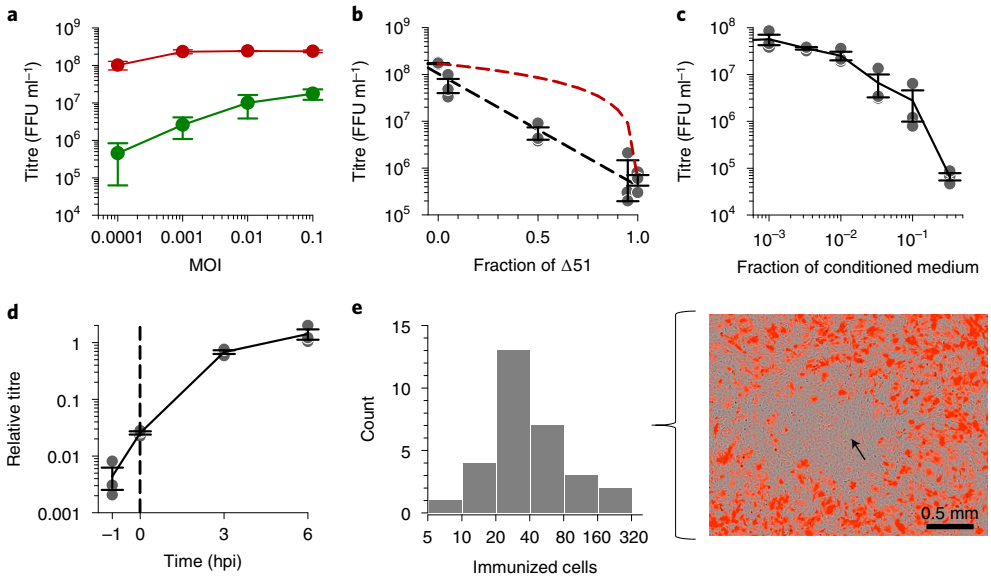

Fig. 2 | Interaction between VSV WT and Δ51 variants. a, Maximal titres of Δ51 (green) and WT (red) in mono-infected cultures at 45 hpi. **b**, Total titres at 45 hpi in cultures infected with Δ51 and WT at different input ratios (MOI = 0.001 FFU cell^{-1}). The black dashed line shows the least-squares linear regression. The red dashed line shows the expected total titre assuming no interaction between the two variants. This was obtained based on the titres reached by pure WT and Δ51 infections as follows: $T(p) = pT_{\Delta 51} + (1-p)T_{WT}$, where T is titre, p is the fraction of Δ51 at inoculation, and $T_{\Delta 51}$ and T_{WT} are the titres reached by pure Δ51 and WT infections, respectively. **c**, The WT titre at 45 hpi in MEFs primed for 1 h with a conditioned medium obtained from a previous Δ51 infection (MOI = 0.001 FFU cell^{-1}). **d**, The time dependence of anti-VSV IFN effects. MEFs were treated with a 1/5 dilution of conditioned medium at the indicated times. All treatments reduced titre significantly (Student's t-test against 1.0: $P = 3.5 \times 10^{-6}$, 2.9×10^{-6} and 0.024 for $t = -1$, 0 and 3 hpi, respectively) except the 6 hpi treatment ($P = 0.290$). The dashed black line indicates the virus innoculation time. In **a**–**d**, error bars indicate the s.e.m. of $n = 3$ independent measures and in **b**–**d**, the three individual data points are also shown. **e**, Range of action of innate immune signalling from single Δ51-infected cells. In the photograph (right), a single cell infected with Δ51 (GFP-positive, apoptotic, shown with arrow) generates a region of cells resistant to the WT virus (lack of red fluorescence). The approximate size of the immunized region was determined by visual inspection. The distribution of immunized cells (left) obtained after analysing 30 images (mean: 54.0 ± 9.6 cells).

undisturbed versus trypsin-treated MEFs. Whereas the Δ51–GFP variant gradually decreased in frequency throughout transfers in undisturbed cells (Pearson correlation (ρ) = −0.808; $P = 0.001$), the situation was reversed in trypsin-treated cells ($\rho = 0.753$; $P = 0.005$; Fig. 4b). Finally, we also performed mixed infections in IFN-null Vero cells. This showed that, in the absence of IFN, the WT was also outcompeted by Δ51 (Supplementary Fig. 3). Overall, this reveals that the WT functions as an altruistic virus ($c > 0$) and that spatial structure ($rb > 0$) is strictly required for selection to favour IFN shutdown. Conversely, Δ51 functions as a social cheater that takes over the population under conditions of low spatial structure even if this reduces population fitness, leading to a 'tragedy of the commons'.

Inference of social evolution parameters

In the absence of spatial structure, $r = 0$ and thus $f_W - f_D = -c$. In contrast, if W and D are fully segregated, $r_W = r_D = r = 1$ and thus $f_W - f_D = f_{W|W} - f_{D|D} = b - c$. By comparing these two scenarios, we determined b and c empirically. For intermediate situations in which the two variants are partially assorted ($0 < r < 1$), we measured f_W and f_D and used the above-estimated b and c to obtain r_D and r_W, since $r_D = (c - f_D)/b$ and $r_W = (f_W + b)/b$. Finally, this allowed us to infer r (Fig. 1). Using fluorescence data (Fig. 3), we calculated log-fitness as $f = \log_{10}[A] - \log_{10}[A_{W|W}]$, where A is the area occupied by infected cells and pure WT infections were taken as reference ($f_{W|W} = 0$). We first focused on 43 hpi data, a time point at which the WT was slightly fitter than Δ51. Assuming that trypsin removed the spatial structure completely, the direct cost of IFN shutdown was $c = 0.394 \pm 0.030$. From pure Δ51 infections, we obtained $f_{D|D} = c - b = -1.221 \pm 0.018$. Hence, $b = 0.393 + 1.221 = 1.615$. From mixed infections, we obtained $f_W = -1.138 \pm 0.060$ and $f_D = -1.236 \pm 0.058$. Thus, the descriptors of spatial structure were $r_D = (c - f_D)/b = 1.009$, $r_W = (f_W + b)/b = 0.295$ and $r = r_D + r_W - 1 = 0.305$. This shows that Δ51 was essentially unaffected by the presence of the WT ($r_D \approx 1$), whereas the WT was strongly inhibited by Δ51 ($r_W < 1$).

To explore the time dependence of the parameters, we repeated our calculations at 20 hpi, a time point at which Δ51 was still fitter than the WT in mixed infections (Fig. 3). From trypsin-treated cultures we obtained $c = 0.806 \pm 0.040$. From pure Δ51 infections, $f_{D|D} = -0.538 \pm 0.001$, giving $b = 1.344$. Hence, during late infection (20–43 hpi) the indirect benefits of IFN shutdown (b) increased, whereas direct costs (c) decreased, favouring the WT variant. This suggests a strengthening of paracrine and autocrine responses in the 20–43 hpi range[26]. From mixed infections we obtained $f_W = -0.942 \pm 0.065$ and $f_D = -0.561 \pm 0.040$ at 20 hpi, thus yielding $r_D = 1.017$, $r_W = 0.299$ and $r = 0.316$. Therefore, r_D, r_W and r showed little variation in this time range, indicating that the spatial structure of infection and immunity were approximately established by 20 hpi.

Metapopulation structure strongly selects for IFN evasion

As shown above, the WT was inhibited by cytokines secreted from Δ51-infected cells. However, viral infections exhibit a marked metapopulation structure in nature in which subpopulations founded by small numbers of transmitted particles remain largely isolated from other subpopulations[29–31]. This occurs between hosts, but also at the intra-host level as a result of tissue or organ compartmentalization[32,33]. To demonstrate the role of metapopulation structure in IFN evasion, we mixed Δ51 and WT variants at an approximately 1:1 ratio and inoculated MEFs subdivided in 96 wells. We used a

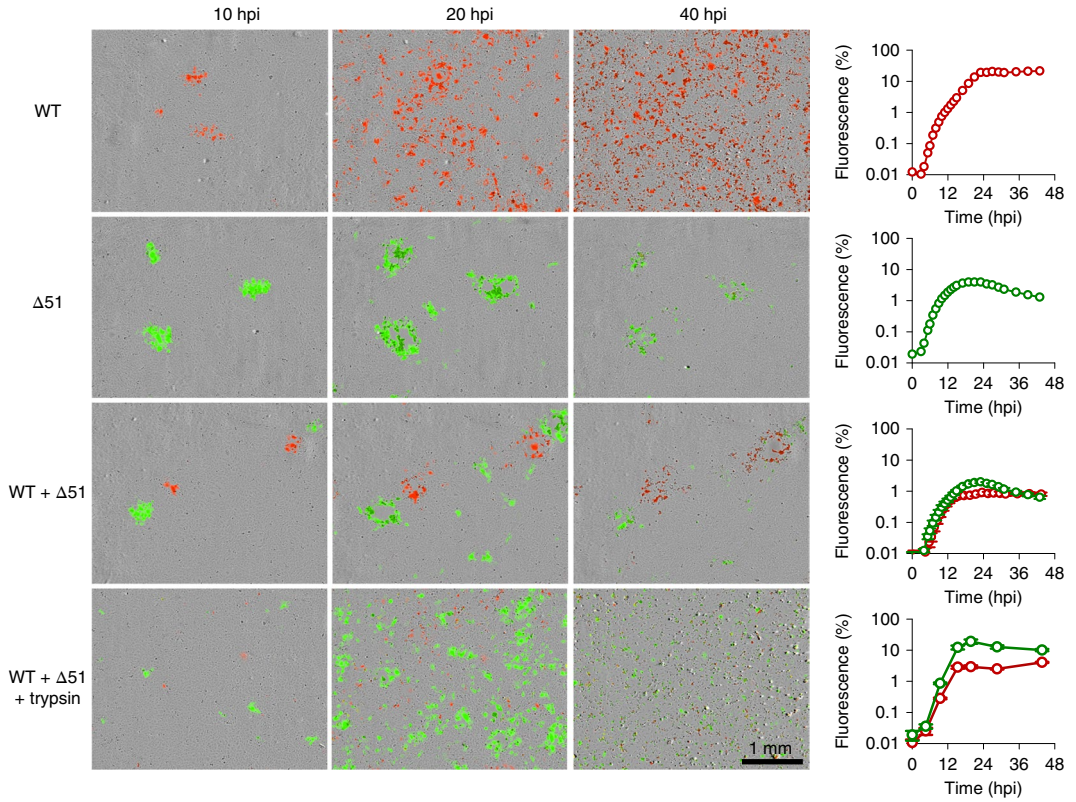

Fig. 3 | Real-time fluorescence microscopy of VSV WT and Δ51 in MEFs. Pure WT–mCherry (red), pure Δ51–GFP (green) and mixed WT–mCherry/Δ51–GFP infections were carried out in the same 12-well dish, which also included mixed WT–mCherry/WT–GFP controls (Supplementary Fig. 2). Left, representative images of three time points. Right, average area occupied by GFP and mCherry signals ($n=2$ replicate wells for pure WT and Δ51 infections; $n=4$ replicates for mixed infections). The graphs were obtained by image analysis of entire culture wells, not just the representative images shown on the left panels. The s.e.m. values (error bars) correspond to the technical error among wells of the same experimental block. Two additional experimental blocks were performed with similar results. For the trypsin treatment (performed at 8 and 24 hpi), fewer data points were analysed because cell detachment prevented imaging at each time point. This treatment was performed in a separate 12-well dish, which included its own controls (Supplementary Fig. 2). The progression of the infection is shown in Supplementary Videos 1–3, and whole-well images are shown in Supplementary Fig. 1.

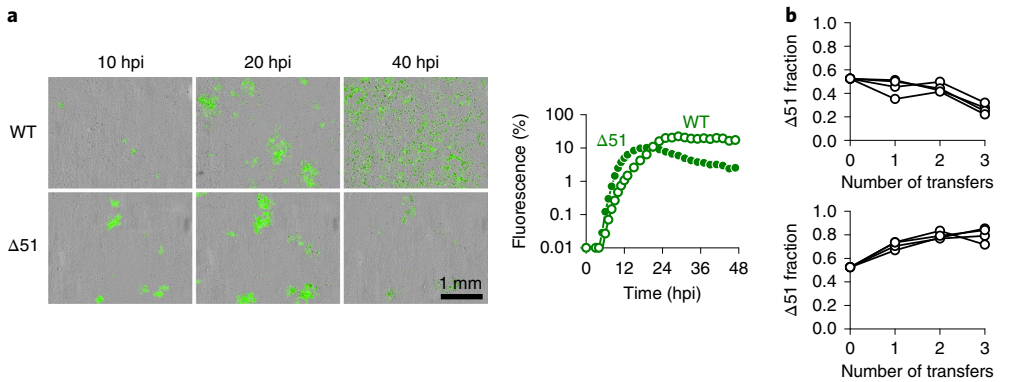

Fig. 4 | Fitness cost of IFN shutdown. a, The spread of pure VSV WT–GFP and pure VSV Δ51–GFP infections. Left, representative images of three time points. Right, average area occupied by the GFP signal ($n=2$ replicate wells). These graphs were obtained by image analysis of entire culture wells, not just the representative images shown on the left panels. Infections were carried out in the same multiwell dish (experimental block) and image acquisition/analysis was performed identically for all wells. Similar results were obtained in another experimental block. **b**, Competition assays between VSV WT–mCherry and Δ51–GFP. Three 48 hpi transfers were performed in undisturbed cells (top) and in cells subjected to trypsin treatment at 8 and 24 hpi (bottom). The Δ51 fraction (GFP/total fluorescent area) after each transfer is shown. Each of the four lines represents one replicate of the competition assay.

limiting dilution of the virus, such that each well typically received 0–2 infectious units. At 48 hpi we determined WT and Δ51 titres. We detected infection in 71/96 wells, of which 20 contained WT only, 35 contained Δ51 only and 16 contained both variants. In wells with mixed infections, the WT reached higher titres than Δ51 (mean log-titres: 5.34 ± 0.30 and 4.13 ± 0.20, respectively; two-tailed

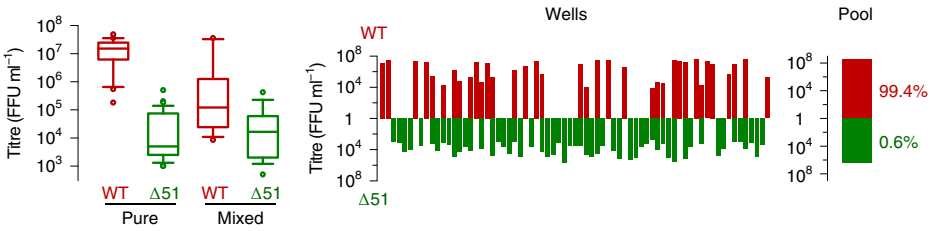

Fig. 5 | Metapopulation structure selects for IFN shutdown. MEFs in a 96-well format were inoculated with a limiting dilution of an approximately 1:1 mix of the WT and a NmAb-resistant Δ51 virus. Titres produced by each variant in each well were determined by the plaque assay. Left, Box plots of the WT and Δ51 titres in wells showing only one variant (pure; $n=20$ for WT and $n=35$ for Δ51) or a mixture of the two variants (mixed; $n=16$). The lower and upper limits of the box indicate the twenty-fifth and seventy-fifth percentiles and the middle line shows the median. Whiskers show the tenth and ninetieth percentiles and outlying points are plotted individually. Middle, titres produced in each individual well. Right, overall WT and Δ51 yield in the metapopulation (sum of all wells).

paired *t*-test: $P<0.001$; Fig. 5), suggesting intrawell spatial structure, as shown above. Nevertheless, the enhanced fitness of the WT was strongly exacerbated in singly infected wells (mean log-titres: 7.00 ± 0.14 and 4.04 ± 0.13 for WT and Δ51, respectively; two-tailed paired *t*-test: $P<0.001$). The WT titre indeed increased by 50-fold in pure infections compared to mixed infections (two-tailed *t*-test: $P<0.001$), whereas the Δ51 titre remained unchanged (two-tailed *t*-test: $P=0.713$). This again confirms that $r_D\approx1$ and $r_W<1$. Pooling all wells, 99.4% of the total progeny was produced by the WT versus 0.6% by Δ51. Hence, a compartmentalized infection with marked founder effects strongly favoured the IFN-blocking virus.

In terms of our model, as the Δ51 virus extracts no benefit from the WT, we can assume a constant log-fitness $f_D=f_{D|D}=c-b$. Assuming no intrawell spatial structure, in mixed groups $f_W-f_D=-c$ (that is $r=0$) and thus $f_W=-b$, whereas in wells containing only WT viruses, $f_W=f_{W|W}=0$. Intrawell spatial structure can be incorporated into the model by noting that the final log yield per well decays linearly with the initial frequency of the Δ51 virus (Fig. 2b; Supplementary Fig. 4). We found that the overall fitness of W increases with the frequency of pure WT infections, which depends inversely on bottleneck size (Supplementary Fig. 4). Hence, transmission bottlenecks should play an important role in the evolution of viral innate immunity evasion.

In vivo validation of the social nature of IFN shutdown

To explore the relevance of our results in vivo, we intranasally inoculated 15 4-week-old Balb/c mice with approximately 10^8 FFU of VSV WT−mCherry. Nine animals succumbed to the infection by days 7−10, showing typical VSV neurological symptoms (altered behaviour, abnormal motility, paralysis). Fluorescence microscopy revealed infection of multiple brain areas, particularly the rostral migratory stream (RMS), thalamus, periventricular areas and spine bulb (Fig. 6a–c). In parallel, we infected 15 animals with approximately 10^8 FFU of WT−mCherry, plus the same amount of Δ51−GFP. Only two animals exhibited typical VSV symptoms (Fisher exact test: $P=0.021$). Of these, one showed limb paralysis but no apparent brain infection at the end-point (day 8). In the other animal, infection was restricted to early viral replication sites such as the olfactory bulb and the anterior RMS (Supplementary Fig. 5), where early IFN signalling is critical for preventing VSV dissemination[34]. Hence, the Δ51 variant interferes with VSV pathogenicity in vivo.

To assess the relative fitness of Δ51 and WT during early infection, we inoculated nine animals with a 1:1 mix as above and killed three animals at 2, 3 and 4 d post inoculation (dpi) to inspect their brains by fluorescence microscopy. We found no evidence of brain infection at 2 dpi. In one 3 dpi animal and two 4 dpi animals, the virus was restricted to the olfactory bulb, which showed multiple infected regions. In these three mice, the infection was clearly dominated by Δ51 (Fig. 6d–f). Exhaustive image analysis of these samples showed that GFP encompassed $87.9\pm7.8\%$ of the total fluorescent area, indicating that Δ51 was initially fitter than the WT (two-tailed *t*-test: $P=0.002$; Supplementary Table 1). The brain of the third 4 dpi animal showed a different pattern, since there was no fluorescence in the olfactory bulb but the WT was found in regions not reached by Δ51, such as the RMS (Supplementary Fig. 6; Supplementary Table 1). Hence, Δ51 spread more efficiently than the WT at early infection sites where it suppressed infection, but the WT occasionally escaped from the inhibitory effects of IFN by reaching more distal regions.

Discussion

We have shown that innate immunity evasion is a social trait in VSV. We first provided a rationale for the social evolution of IFN shutdown in viruses based on a partition of viral fitness according to social neighbourhood. Then, we demonstrated experimentally that cytokines produced by cells infected with VSV Δ51 strongly inhibit the growth of nearby viruses, including the IFN-suppressing WT. Furthermore, we found that IFN shutdown is costly because Δ51 outcompetes the WT when both viruses share the same neighbourhood, that is, in non-assorted populations. Therefore, the evolution of IFN shutdown is critically dependant on spatial structure, which allows the WT to avoid the interference exerted by the Δ51 variant.

Previous work reported substitutions in the M protein of VSV populations passaged in IFN-deficient cells, including M51 but also S32, Y61, P120, L123 and V221[35–39]. Molecular characterization of the L123W variant revealed that it impairs the ability of the VSV protein M to block IFN production[40] and this mutant was found to interfere with WT VSV pathogenicity in vivo[41]. Furthermore, substitutions P120A and L123W were shown to confer accelerated growth in IFN-deficient cells[42]. Therefore, our findings with the Δ51 mutation probably apply to other VSV variants. Considering the fast mutational supply of RNA viruses, the appearance of IFN-stimulating cheater viruses may thus be relatively common. This is suggested by the observation that natural VSV isolates vary greatly in their ability to stimulate IFN[35,43]. Such cheaters could potentially reach high frequencies transitorily, but their ability to invade populations should be curtailed by spatial structure, which is present at many levels including infection foci within tissues, organ compartmentalization and among individual hosts. In future work, this could be investigated by deep-sequencing natural viral populations at the intra-host level.

VSV WT and Δ51 obey a yield/rate fitness trade-off because Δ51 initially replicates faster than the WT but reaches a lower final titre. Analogous trade-offs have been reported in widely different biological systems, such as microbial metabolic pathways in which they also lead to cooperation/cheating dilemmas[44]. However, in

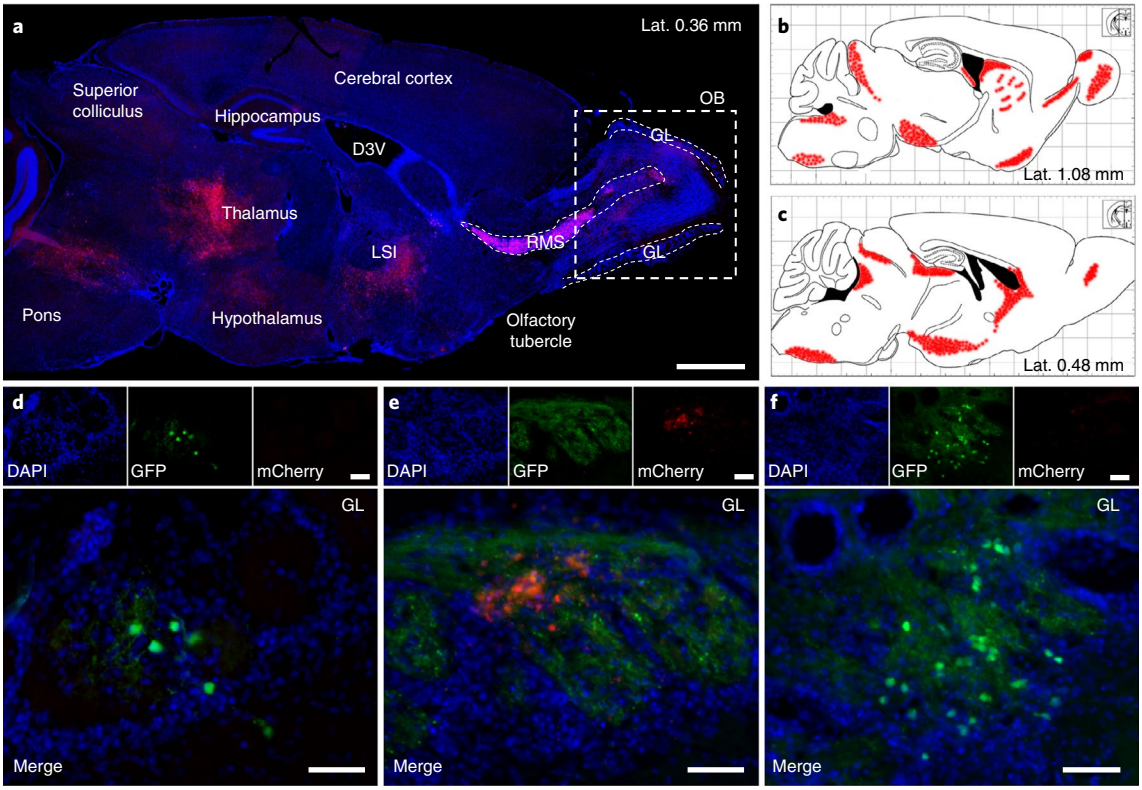

Fig. 6 | Fluorescence microscopy of VSV-infected mouse brains. a, Brain full sagittal section (except cerebellum) of a mouse succumbing to an infection by VSV WT−mCherry (red nuclei stained with blue 4,6-diamidino-2-phenylindole (DAPI)). The dashed white box indicates the olfactory bulb (OB). Scale bar, 1 mm. Lat., lateral; D3V, dorsal third ventricle; LSI, lateral septal nucleus intermediate part. **b**,**c**, Schematic representations of the infection pattern observed in two additional, parallel sections. Red colouring indicates infected areas. Given that animals were inoculated intranasally, the observed pattern is consistent with primary infection of the OB glomerular layer (GL) originating from olfactory axons and spreading along the RMS. Isolated infected areas were also found in the olfactory tubercle. The infection may have progressed from the RMS towards the lateral ventricles, producing infected areas adjacent to the ventricular walls (the lateral septal nucleus, the striatum adjacent to the anterior region of the lateral ventricle and the hippocampus adjacent to the posterior ventricle). Hence, the ventricular system probably acted as a route for disseminating the infection towards the thalamus and hypothalamus. The thalamus appears as another major infection site, from which the virus may have reached the spinal cord, producing paralysis. Examination of the brains from two additional animals inoculated with WT−mCherry showed similar infection patterns. The OB of a pure WT infection and OB/RMS regions of a mixed infection are shown in Supplementary Fig. 5. **d**–**f**, Individual infected regions in the OB glomerular layer of $n = 3$ mice infected with a 1:1 mix of WT−mCherry and Δ51−GFP, one at 3 dpi (**d**) and two at 4 dpi (**e**,**f**). Scale bars, 50 μm. In these three animals, no signs of infection were found in the rest of the brain. Quantitation of the area occupied by Δ51−GFP and WT−mCherry is shown in Supplementary Table 1.

our system, the cheater stimulates the release of an inhibitor that reduces the fitness of all its neighbours. This could be relevant to other fast-growth processes producing toxic by-products, for example ethanol release during yeast fermentation[45]. An open question is whether such 'pollutants' could promote a co-evolution process whereby cooperators evolve resistance to the inhibitor.

Future work may elucidate the mechanistic basis of IFN shutdown costs. At present, we can only speculate that, in VSV, such costs may stem from the multifunctional nature of the M protein. In addition to blocking host gene expression, the M protein is a structural component of the virion. Hence, directing M proteins to block mRNA export might reduce the amount of protein available for virion assembly. As most RNA virus proteins are highly multifunctional, similar costs could apply to immunity suppressors of other viruses. Alternatively, host gene expression shutdown might reduce the ability of the virus to use cellular factors exported from the nucleus, or trigger apoptosis prematurely.

IFNs have been administered systemically to patients as a non-specific antiviral. Delivery of IFN-stimulating, attenuated viruses might achieve a response that is more selectively directed towards viral replication sites, potentially increasing efficacy. VSV provides a safe and flexible platform for oncolytic virotherapy[46] and has also been used for vaccine design[47]. In principle, VSV thus offers a good model for developing 'antiviral virotherapy' strategies based on IFN stimulation. Social evolution principles may prove helpful for achieving this goal, as also suggested for bacteria[48].

Methods

Virus. VSV WT−mCherry, WT−GFP and Δ51−GFP were obtained from an infectious cDNA clone[49] kindly provided by V. Z. Grdzelishvili (University of North Carolina). Colours were used to track the WT and Δ51 variants. In the event of a reversion of the Δ51 mutation, the association between colours and variants would be lost, but three-base deletions are highly unlikely to revert in the short term. In addition, because VSV recombines very infrequently, each variant was stably linked to its corresponding fluorescent reporter.

Cells. MEFs from C57BL/6 mice were isolated as previously described[50] and provided by C. Rivas (Universidad de Santiago de Compostela). BHK-21 (CCL-10) and Vero (CCL-81) cells were purchased from the American Type Culture Collection (ATCC; reference numbers indicated in parentheses). All cells were cultured in DMEM buffer supplemented with 10% fetal bovine serum (FBS) at 37 °C in a 5% CO_2 humidified incubator and tested mycoplasma-negative by PCR.

Viral titration. BHK-21 cells were inoculated with various dilutions of the virus, incubated for 45 min (37 °C; 5% CO_2) and overlaid with DMEM supplemented with 2% FBS containing 0.6% agar. After 20–24 h, cells were fixed with 10% formaldehyde, stained with 2% crystal violet and used for counting plaques.

Automated real-time fluorescence microscopy. Confluent MEFs in 12-well dishes were inoculated with VSV and kept in an IncuCyte S3 Live-Cell Analysis System (Essen BioScience) at 37 °C and 5% CO_2. Images were acquired using phase contrast, green and red channels at ×4 magnification. For background correction, raw images were subjected to a top-hat transform using a 100 µm disk. To measure the area occupied by the fluorescence signal, images were segmented by defining a grey-scale intensity threshold such that the fluorescent areas of WT−GFP and WT−mCherry controls were similar (Supplementary Fig. 2). Once defined, the image analysis parameters were kept constant and identical for all experiments. All images share the same saturation values for each channel. For trypsin treatments, the supernatant was collected, the cells were washed with PBS, detached with trypsin, spun and washed to remove the trypsin, resuspended in the original supernatant and added back to the culture dishes.

Infection and titration in a subdivided MEF population. Confluent MEFs in a 96-well dish were inoculated with a limiting dilution of VSV WT and a NmAb-resistant Δ51 mutant mixed at an approximately 1:1 ratio. Cultures were incubated for 48 h and supernatants were collected to perform plaque assays in the absence/presence of NmAb, which allowed us to determine the titre of each variant in each well.

Extraction of cytokine-containing medium. Conditioned medium was obtained by infecting a confluent MEF monolayer with VSV Δ51 at an MOI of ~3 FFU cell^{-1} and collecting the infection medium at 24 hpi. The supernatant was centrifuged at 5,000*g* for 10 min to remove cellular debris and cleared of virions through a 0.05 µm cellulose filter (MF-Millipore; VMWP02500). The undiluted resulting medium was subjected to the plaque assay to verify the absence of infectious particles.

Reverse transcription (RT)−qPCR. Infected MEFs in 6-well dishes were used for total RNA extraction by the acid guanidinium−thiocyanate−phenol−chloroform method (Invitrogen). Total RNA concentrations were adjusted to 150 ng µl^{-1} and subjected to RT using SuperScript IV (Invitrogen) and specific primers for either mouse Mx2 mRNA (5′-TGGAGTCGGATTGACATCTCTG) or β-actin mRNA (5′-CAGAGGCATACAGGGACAGC). Reverse transcription reactions were carried out at 55 °C following the manufacturer's instructions. The qPCRs were performed by the SYBR Green method (Agilent) using specific primers for Mx2 (5′-ACACGGTCACTGAAATTGTACG, 5′-TCATCTTTTCACGGTTGGCTT) or β-actin mRNA (5′-CTGGCACCACACCTTCTACA, 5′-TCATCTTTTCACGGTTGGCTT) under the following cycling conditions: 95 °C for 3 min, and 40 cycles of 95 °C for 15 s and 60 °C for 20 s. RT−qPCR assays were performed in triplicate.

ELISA. Supernatants from 24-well dishes were collected, diluted 1:5 and assayed in triplicate using an IFN-β ELISA kit following the manufacturer's instructions (Pierce).

Mouse infections. VSV WT−mCherry and Δ51−GFP were purified in an iodixanol gradient by high-speed centrifugation and used for intranasal inoculation of 4-week-old Balb/c (Charles River) females with approximately $0.5–1.0 \times 10^8$ FFU of pure WT, or a mixture of WT and Δ51 ($0.5–1.0 \times 10^8$ FFU each). The inoculum was administered by aspiration of 10 µl through the nostrils. Animals infected with Δ51/WT mixes or pure WT were kept in separate cages and inspected daily for symptoms of infection. Animals showing VSV-induced brain damage symptoms such as severely altered behaviour, abnormal motility or paralysis as well as other end-point criteria were euthanized by cervical dislocation or perfused for microscopy analysis. This procedure was approved by the Biosafety Committee and the Animal Welfare Ethics Committee of the Universitat de València and relevant authorities (procedure 2018/VSC/PEA/0029).

Brain fluorescence microscopy. Animals were perfused intracardiacally with NaCl 0.9% followed by 4% paraformaldehyde. Brains were extracted and incubated overnight in the same fixator, washed in phosphate buffer and cryopreserved in sucrose 30%. We obtained 25 µm sections in a Leica cryostat, which were stained with DAPI and mounted using Fluorsave reagent (VWR). Sections were analysed under a Leica DMi8 fluorescence microscope and the images were captured with a Leica DFC 3000 G camera assisted with proprietary LasX software. To measure the area occupied by GFP- and mCherry-positive cells in the olfactory bulbs, we examined five infected regions per animal, which constituted an exhaustive analysis of the infection. Images were subjected to background correction using a 50 µm (radius) rolling ball, corrected for brightness and contrast, and binarized to measure the fluorescence-positive area. For some images, a two-pixel radius median filter and an erode/dilate process were needed to properly fit the binary mask to the actual fluorescence signal. This analysis was performed with ImageJ/Fiji software.

Reporting Summary. Further information on research design is available in the Nature Research Reporting Summary linked to this article.

Data availability

No restrictions apply to data availability. Relevant data are provided in the manuscript and the Supplementary Information. All data are available from the corresponding author upon request. No new protein, DNA or RNA sequence data, macromolecular structures, crystallographic data or microarray data requiring deposition in public repositories were produced.

Received: 25 September 2018; Accepted: 18 January 2019;
Published online: 04 March 2019

References

1. Nowak, M. A. Five rules for the evolution of cooperation. *Science* **314**, 1560–1563 (2006).
2. Fletcher, J. A. & Doebeli, M. A simple and general explanation for the evolution of altruism. *Proc. Biol. Sci.* **276**, 13–19 (2009).
3. Gardner, A., West, S. A. & Wild, G. The genetical theory of kin selection. *J. Evol. Biol.* **24**, 1020–1043 (2011).
4. Díaz-Munoz, S. L., Sanjuán, R. & West, S. Sociovirology: conflict, cooperation, and communication among viruses. *Cell Host Microbe* **22**, 437–441 (2017).
5. Turner, P. E. & Chao, L. Prisoner's dilemma in an RNA virus. *Nature* **398**, 441–443 (1999).
6. Skums, P., Bunimovich, L. & Khudyakov, Y. Antigenic cooperation among intrahost HCV variants organized into a complex network of cross-immunoreactivity. *Proc. Natl Acad. Sci. USA* **112**, 6653–6658 (2015).
7. Erez, Z. et al. Communication between viruses guides lysis-lysogeny decisions. *Nature* **541**, 488–493 (2017).
8. Borges, A. L. et al. Bacteriophage cooperation suppresses CRISPR-Cas3 and Cas9 immunity. *Cell* **174**, 917–925 (2018).
9. Xue, K. S., Hooper, K. A., Ollodart, A. R., Dingens, A. S. & Bloom, J. D. Cooperation between distinct viral variants promotes growth of H3N2 influenza in cell culture. *eLife* **5**, e13974 (2016).
10. Leggett, H. C., Brown, S. P. & Reece, S. E. War and peace: social interactions in infections. *Phil. Trans. R. Soc. B* **369**, 20130365 (2014).
11. Xavier, J. B. Sociomicrobiology and pathogenic bacteria. *Microbiol. Spectr.* https://doi.org/10.1128/microbiolspec.VMBF-0019-2015 (2016).
12. Ivashkiv, L. B. & Donlin, L. T. Regulation of type I interferon responses. *Nat. Rev. Immunol.* **14**, 36–49 (2014).
13. Fensterl, V., Chattopadhyay, S. & Sen, G. C. No love lost between viruses and interferons. *Annu. Rev. Virol.* **2**, 549–572 (2015).
14. García-Sastre, A. Ten strategies of interferon evasion by viruses. *Cell Host Microbe* **22**, 176–184 (2017).
15. Coccia, E. M. & Battistini, A. Early IFN type I response: learning from microbial evasion strategies. *Semin. Immunol.* **27**, 85–101 (2015).
16. Lion, S., Jansen, V. A. & Day, T. Evolution in structured populations: beyond the kin versus group debate. *Trends Ecol. Evol.* **26**, 193–201 (2011).
17. Birch, J. Kin selection, group selection, and the varieties of population structure. *Brit. J. Phil. Sci.* https://doi.org/10.1093/bjps/axx028 (2018).
18. Lehtonen, J. Multilevel selection in kin selection language. *Trends Ecol. Evol.* **31**, 752–762 (2016).
19. Marshall, J. A. Group selection and kin selection: formally equivalent approaches. *Trends Ecol. Evol.* **26**, 325–332 (2011).
20. West, S. A., Griffin, A. S., Gardner, A. & Diggle, S. P. Social evolution theory for microorganisms. *Nat. Rev. Microbiol.* **4**, 597–607 (2006).
21. O'Brien, S., Luján, A. M., Paterson, S., Cant, M. A. & Buckling, A. Adaptation to public goods cheats in *Pseudomonas aeruginosa*. *Proc. Biol. Sci.* **284**, 20171089 (2017).
22. Jin, Z. et al. Conditional privatization of a public siderophore enables *Pseudomonas aeruginosa* to resist cheater invasion. *Nat. Commun.* **9**, 1383 (2018).
23. Rajani, K. R. et al. Complexes of vesicular stomatitis virus matrix protein with host Rae1 and Nup98 involved in inhibition of host transcription. *PLoS Pathog.* **8**, e1002929 (2012).
24. Quan, B., Seo, H. S., Blobel, G. & Ren, Y. Vesiculoviral matrix (M) protein occupies nucleic acid binding site at nucleoporin pair (Rae1 * Nup98). *Proc. Natl Acad. Sci. USA* **111**, 9127–9132 (2014).
25. Stojdl, D. F. et al. VSV strains with defects in their ability to shutdown innate immunity are potent systemic anti-cancer agents. *Cancer Cell* **4**, 263–275 (2003).
26. Voigt, E. A., Swick, A. & Yin, J. Rapid induction and persistence of paracrine-induced cellular antiviral states arrest viral infection spread in A549 cells. *Virology* **496**, 59–66 (2016).
27. Howat, T. J., Barreca, C., O'Hare, P., Gog, J. R. & Grenfell, B. T. Modelling dynamics of the type I interferon response to in vitro viral infection. *J. R. Soc. Interface* **3**, 699–709 (2006).
28. Samuel, C. E. & Knutson, G. S. Mechanism of interferon action. Kinetics of decay of the antiviral state and protein phosphorylation in mouse fibroblasts treated with natural and cloned interferons. *J. Biol. Chem.* **257**, 6 (1982).
29. Zwart, M. P. & Elena, S. F. Matters of size: genetic bottlenecks in virus infection and their potential impact on evolution. *Annu. Rev. Virol.* **2**, 161–179 (2015).

30. Gutiérrez, S., Michalakis, Y. & Blanc, S. Virus population bottlenecks during within-host progression and host-to-host transmission. *Curr. Opin. Virol.* **2**, 546–555 (2012).
31. McCrone, J. T. & Lauring, A. S. Genetic bottlenecks in intraspecies virus transmission. *Curr. Opin. Virol.* **28**, 20–25 (2018).
32. Richard, M., Herfst, S., Tao, H., Jacobs, N. T. & Lowen, A. C. Influenza A virus reassortment is limited by anatomical compartmentalization following co-infection via distinct routes. *J. Virol.* https://doi.org/10.1128/JVI.02063-17 (2017).
33. Salemi, M. & Rife, B. Phylogenetics and phyloanatomy of HIV/SIV intra-host compartments and reservoirs: the key role of the central nervous system. *Curr. HIV Res.* **14**, 110–120 (2016).
34. Detje, C. N. et al. Local type I IFN receptor signaling protects against virus spread within the central nervous system. *J. Immunol.* **182**, 2297–2304 (2009).
35. Francoeur, A. M., Poliquin, L. & Stanners, C. P. The isolation of interferon-inducing mutants of vesicular stomatitis virus with altered viral P function for the inhibition of total protein synthesis. *Virology* **160**, 236–245 (1987).
36. Novella, I. S., Hershey, C. L., Escarmís, C., Domingo, E. & Holland, J. J. Lack of evolutionary stasis during alternating replication of an arbovirus in insect and mammalian cells. *J. Mol. Biol.* **287**, 459–465 (1999).
37. Cuevas, J. M., Elena, S. F. & Moya, A. Molecular basis of adaptive convergence in experimental populations of RNA viruses. *Genetics* **162**, 533–542 (2002).
38. Remold, S. K., Rambaut, A. & Turner, P. E. Evolutionary genomics of host adaptation in vesicular stomatitis virus. *Mol. Biol. Evol.* **25**, 1138–1147 (2008).
39. Morita, K., Vanderoef, R. & Lenard, J. Phenotypic revertants of temperature-sensitive M protein mutants of vesicular stomatitis virus: sequence analysis and functional characterization. *J. Virol.* **61**, 256–263 (1987).
40. Brun, J. et al. Identification of genetically modified Maraba virus as an oncolytic rhabdovirus. *Mol. Ther.* **18**, 1440–1449 (2010).
41. Furió, V. et al. Relationship between within-host fitness and virulence in the vesicular stomatitis virus: correlation with partial decoupling. *J. Virol.* **86**, 12228–12236 (2012).
42. Sanjuán, R., Moya, A. & Elena, S. F. The distribution of fitness effects caused by single-nucleotide substitutions in an RNAvirus. *Proc. Natl Acad. Sci. USA* **101**, 8396–8401 (2004).
43. Marcus, P. I., Rodríguez, L. L. & Sekellick, M. J. Interferon induction as a quasispecies marker of vesicular stomatitis virus populations. *J. Virol.* **72**, 542–549 (1998).
44. Pfeiffer, T., Schuster, S. & Bonhoeffer, S. Cooperation and competition in the evolution of ATP-producing pathways. *Science* **292**, 504–507 (2001).
45. Stanley, D., Bandara, A., Fraser, S., Chambers, P. J. & Stanley, G. A. The ethanol stress response and ethanol tolerance of *Saccharomyces cerevisiae*. *J. Appl. Microbiol.* **109**, 13–24 (2010).
46. Hastie, E. & Grdzelishvili, V. Z. Vesicular stomatitis virus as a flexible platform for oncolytic virotherapy against cancer. *J. Gen. Virol.* **93**, 2529–2545 (2012).
47. Clarke, D. K. et al. Live virus vaccines based on a vesicular stomatitis virus (VSV) backbone: standardized template with key considerations for a risk/benefit assessment. *Vaccine* **34**, 6597–6609 (2016).
48. Brown, S. P., West, S. A., Diggle, S. P. & Griffin, A. S. Social evolution in micro-organisms and a Trojan horse approach to medical intervention strategies. *Phil. Trans. R. Soc. B* **364**, 3157–3168 (2009).
49. Lawson, N. D., Stillman, E. A., Whitt, M. A. & Rose, J. K. Recombinant vesicular stomatitis viruses from DNA. *Proc. Natl Acad. Sci. USA* **92**, 4477–4481 (1995).
50. Palmero, I. & Serrano, M. Induction of senescence by oncogenic Ras. *Methods Enzymol.* **333**, 247–256 (2001).

Acknowledgements

We thank I. Noguera for technical assistance with the animal experiments, J. M. Cuevas, R. Garijo and I. Andreu-Moreno for help with the experimental set up, V. Grdzelishvili for the VSV clones, C. Rivas for the MEFs, and S. West and P. Carazo for helpful discussions. This work was funded by ERC Consolidator Grant 724519 Vis-a-Vis to R.S. P.D.-C. was also funded by a Juan de la Cierva Incorporación postdoctoral contract from the Spanish MINECO.

Author contributions

P.D.-C. performed the cell culture experiments. E.S.-O. contributed to designing the model. M.D.-M. performed the animal experiments. R.S. conceived the study, formulated the model, analysed the data and wrote the manuscript.

Competing interests

The authors declare no competing interests.

Additional information

Supplementary information is available for this paper at https://doi.org/10.1038/s41564-019-0379-8.

Reprints and permissions information is available at www.nature.com/reprints.

Correspondence and requests for materials should be addressed to R.S.

Publisher's note: Springer Nature remains neutral with regard to jurisdictional claims in published maps and institutional affiliations.

nature research

Corresponding author(s): Rafael Sanjuán

Reporting Summary

Nature Research wishes to improve the reproducibility of the work that we publish. This form provides structure for consistency and transparency in reporting. For further information on Nature Research policies, see Authors & Referees and the Editorial Policy Checklist.

Statistical parameters

When statistical analyses are reported, confirm that the following items are present in the relevant location (e.g. figure legend, table legend, main text, or Methods section).

n/a	Confirmed	
☐	☒	The exact sample size (*n*) for each experimental group/condition, given as a discrete number and unit of measurement
☐	☒	An indication of whether measurements were taken from distinct samples or whether the same sample was measured repeatedly
☐	☒	The statistical test(s) used AND whether they are one- or two-sided *Only common tests should be described solely by name; describe more complex techniques in the Methods section.*
☒	☐	A description of all covariates tested
☒	☐	A description of any assumptions or corrections, such as tests of normality and adjustment for multiple comparisons
☐	☒	A full description of the statistics including central tendency (e.g. means) or other basic estimates (e.g. regression coefficient) AND variation (e.g. standard deviation) or associated estimates of uncertainty (e.g. confidence intervals)
☐	☒	For null hypothesis testing, the test statistic (e.g. *F*, *t*, *r*) with confidence intervals, effect sizes, degrees of freedom and *P* value noted *Give P values as exact values whenever suitable.*
☒	☐	For Bayesian analysis, information on the choice of priors and Markov chain Monte Carlo settings
☒	☐	For hierarchical and complex designs, identification of the appropriate level for tests and full reporting of outcomes
☐	☒	Estimates of effect sizes (e.g. Cohen's *d*, Pearson's *r*), indicating how they were calculated
☐	☒	Clearly defined error bars *State explicitly what error bars represent (e.g. SD, SE, CI)*

Our web collection on statistics for biologists may be useful.

Software and code

Policy information about availability of computer code

Data collection	Image data were acquired with IncuCyte S2 proprietary software.
Data analysis	Statistical analyses were performed using SPSS v24.

For manuscripts utilizing custom algorithms or software that are central to the research but not yet described in published literature, software must be made available to editors/reviewers upon request. We strongly encourage code deposition in a community repository (e.g. GitHub). See the Nature Research guidelines for submitting code & software for further information.

Data

Policy information about availability of data

All manuscripts must include a data availability statement. This statement should provide the following information, where applicable:

- Accession codes, unique identifiers, or web links for publicly available datasets
- A list of figures that have associated raw data
- A description of any restrictions on data availability

The sequence of the virus is publicly available (accession provided). No restrictions apply to data availability. All figures report raw data, except Fig 2a, Fig 3, Fig 4a, Fig S2, and Fig S3 which report averaged data (as indicated in legends). If requested, all raw data will be provided in Excel format.

Field-specific reporting

Please select the best fit for your research. If you are not sure, read the appropriate sections before making your selection.

☒ Life sciences ☐ Behavioural & social sciences ☐ Ecological, evolutionary & environmental sciences

For a reference copy of the document with all sections, see nature.com/authors/policies/ReportingSummary-flat.pdf

Life sciences study design

All studies must disclose on these points even when the disclosure is negative.

Sample size	A default sample size of 3 was used. Higher (n= 4 or higher) or lower (n=2) sizes were used in some cases depending on the observed experimental variance and on feasability.
Data exclusions	No data were excluded.
Replication	Replicates are shown in the manuscript.
Randomization	No randomization was required in the cell culture assays. In the animal infections, we chose to keep the animals receiving the two treatments (WT alone vs WT+D51) in separate cages to avoid transmission/contamination. Three cages were used per treatment (5 animals/cage, 15 animals), and their location was randomized.
Blinding	Blinding was not relevant to the cell culture assays because data acquisition was automatized. Blinding was applied to animal infections.

Reporting for specific materials, systems and methods

Materials & experimental systems

n/a	Involved in the study
☒	☐ Unique biological materials
☐	☒ Antibodies
☐	☒ Eukaryotic cell lines
☒	☐ Palaeontology
☐	☒ Animals and other organisms
☒	☐ Human research participants

Methods

n/a	Involved in the study
☒	☐ ChIP-seq
☒	☐ Flow cytometry
☒	☐ MRI-based neuroimaging

Antibodies

Antibodies used	A non-commercial anti VSV-G antibody (hybridoma supernatant) was used. This antibody was originally produced by Dr. JJ Holland and is described extensively in the literature (references will be provided).
Validation	Validation is solely based on viral neutralization, as determined by standard plaque assays. The Mab was not used for microscopy or flow cytometry.

Eukaryotic cell lines

Policy information about cell lines

Cell line source(s)	MEFs from C57BL/6 mice were isolated from animals and provided by Dr. Carmen Rivas (Universidad de Santiago de Compostela, Spain). BHK-21 (CCL-10) and Vero (CCL-81) cells were purchased from the American Type Culture Collection (ATCC, reference number indicated in parentheses).
Authentication	MEFs were not authenticated, as they were primarily obtained from authenticated animals. Commercial cell lines are to be authenticated by ATCC.
Mycoplasma contamination	All cells tested negative by PCR.
Commonly misidentified lines (See ICLAC register)	None.

Animals and other organisms

Policy information about studies involving animals; ARRIVE guidelines recommended for reporting animal research

Laboratory animals	Four-week-old Balb/c (Charles River) females
Wild animals	None.
Field-collected samples	None.